Improved Adhesion of TiO_2-Based Multilayer Coating on HDPE and Characterization of Photocatalysis

Jussi Kasanen, Mika Suvanto, Tuula T. Pakkanen

Department of Chemistry, University of Joensuu, P.O. Box 111, FIN-80101 Joensuu, Finland

Received 28 October 2009; accepted 11 June 2010
DOI 10.1002/app.32948
Published online 27 August 2010 in Wiley Online Library (wileyonlinelibrary.com).

ABSTRACT: Multilayered photocatalytic TiO_2-based coating was prepared by spin coating on a high-density polyethylene (HDPE) substrate. The multilayered coating consisted of a polyurethane (PU) barrier layer and two layers of TiO_2 nanoparticles bound with PU. The adhesion between the HDPE substrate and protective PU coating was enhanced by oxygen plasma treatment of the substrate. The improved adhesion contributed to the photocatalytic degradation of palmitic acid. Long-term activity of the photocatalytic coating in degradation of palmitic acid under UV illumination was followed by FTIR-ATR. The catalytic activity of the coating was maintained in three identical cycles where palmitic acid was added and UV-irradiated for 6 h. According to FTIR measurements, the palmitic acid was almost completely decomposed after 6 h, but gas chromatography (GC) analysis showed total decomposition to require 12 h UV illumination ($\sim$ 97% of palmitic acid decomposed in 12 h). Study of the degradation of palmitic acid by GC as a function of time indicated that the degradation kinetics was pseudofirst order, and the rate constant obtained was 0.31 h^{-1}. © 2010 Wiley Periodicals, Inc. J Appl Polym Sci 119: 2235–2245, 2011

Key words: coatings; FTIR; photochemistry; polyethylene (PE)

INTRODUCTION

Research on semiconductor photocatalysis with titanium dioxide as catalyst, has intensified ever since 1972, when Fujishima and Honda first described the UV-induced photocatalysis of water splitting to produce hydrogen with the help of titanium dioxide.[1,2] Titanium dioxide is the most promising catalyst for practical applications of photocatalysis because of its unique properties: chemical and physical stability, relatively low band gap, high photocatalytic efficiency, and low cost.[3–8] Titanium dioxide is produced in large quantities and in several particle sizes for different applications. Typically, small particles (nanoparticles) are used in photocatalytic applications because of large specific surface area and larger particles (micrometer size) as pigments and filling materials.[9–11] Pigment crystals (about 200 nm) scatter visible light most efficiently[10] but in case of ultrafine pigment particles (about 2–50 nm) the light scattering power diminishes and the system becomes transparent in the visible range.[12] Ultrafine titanium dioxide pigments are used for UV-protection e.g., in coatings (lacquers and paints), polymers, and sunscreens.[12–14]

Photocatalytic titanium dioxide (TiO_2) can be combined with a variety of materials, such as ceramics,[15] glass,[16–18] metal,[19] polymer,[20–28] textiles,[29,30] and wood,[31] for use in air and water purification and self-cleaning and antifogging applications.[32] The photocatalytic effect exploited in these applications depends on the highly oxidative radicals and oxidative compounds that are formed during light-induced photocatalysis. The oxidative species include hydroxyl radical (HO[chemp]) and hydrogen peroxide (H_2O_2). Titanium dioxide photocatalysis degrades organic materials and organic waste both in air and in solution. In addition, TiO_2 has an antibacterial effect.[33]

Achieving a large surface area means that the particle size of TiO_2 must be correspondingly small (nanoparticles). TiO_2 catalyst is typically immobilized on inorganic oxide substrates, but rarely on polymer surfaces because photocatalysis tends to degrade the polymer.[34,35] The main ways to attach TiO_2 particles to polymer substrates are physical and chemical fixing.[20–28,36] In the case of polyethylene (PE), fixing methods include ironing of PE film sprinkled with TiO_2 powder,[21] embedding PE film into TiO_2 suspension and heating,[22,23] and hot pressing.[24] TiO_2 can also be bound to polymer substrate with other polymers such as silicon-based liquid adhesives.[36] Electrostatic interactions can be utilized to fix TiO_2 particles to PE-based copolymers when the copolymers have been grafted with reactive functional groups like maleic anhydride or 4-vinyl pyridine/acryl amide.[26,27]

Depending on the application, the polymer substrate can be protected with a barrier layer, on which TiO_2 lies without direct contact to the polymer.[27,37–39]

Correspondence to: T. T. Pakkanen (tuula.pakkanen@joensuu.fi).

Earlier,[40] we used thermally cured polyurethane as a barrier layer for the protection of a HDPE substrate. TiO_2 nanoparticles were then fixed on top of the barrier with use of diluted polyurethane dispersion as binding agent. Commercially available waterborne polyurethane dispersion is easy to use and economical. It can be diluted merely with water, without harmful solvents, and since curing is done thermally no catalyst is required.

In this study, we developed further our multilayer TiO_2 nanoparticle (Degussa P25) coating on HDPE[40] with the aim of improving the adhesion between the protective polyurethane barrier layer and the HDPE substrate and increasing the photocatalytic efficiency of the multilayer coating. To determine whether the photocatalytic activity of the coating was preserved after the first cycle, and thereby to evaluate the long-term activity of the coating, we repeated the UV-degradation cycle with successive fatty acid loadings. The decomposition kinetics of palmitic acid was another point of interest.

EXPERIMENTAL

Preparation and pretreatment of substrate material

The thermoplastic resin used as substrate material was high-density polyethylene (CG8410, Borealis, Porvoo, Finland), which is a suitable grade for extrusion coating. Granules were melted and mixed in a DSM Midi 2000 extruder and injection molded to sample disks in a DSM microinjection molding machine (Geleen, Netherlands). Temperatures were 210°C (melt temperature ~ 203°C) for the extruder and 215°C for the injection molding cylinder. Mold temperature was kept at 40°C, and air pressure of the injection piston was 3.5 bar. The final prepared sample disks were 2.4 cm in diameter and ~ 1.5 mm thick.

After injection molding, sample disks were plasma treated. Samples were etched by reactive ion etching with use of oxygen as reactive etching gas. Reactive ion etching was done with a March CS 1701 Reactive Ion Etching system (Concord, California). Working pressure in the chamber was ~ 80 mTorr, oxygen flow was 20 SCCM, and the etching power was set to 200 W for 30 s.

Preparation of photocatalytic multilayer coating

Preparation of the multilayer coating consisted of three steps: (1) coating of the plasma treated HDPE substrate with a protective layer, (2) preparation of two TiO_2 layers, and (3) fixing of TiO_2 particles with binding agent. In addition, some of the samples were plasma treated after curing of the binding agent. Spin coating parameters are reported in Table I.

TABLE I
Spin Coating Parameters for the Different Stages of Preparation of Photocatalytic Coating

Preparation stage	Spinning [time (s)/ rotation speed (rpm)]
Diluted PU dispersion (1 : 1) (protective PU)	5/800, 10/3000, 15/6000
TiO_2/water suspension (2 wt % TiO_2)	5/800, 10/2200
Diluted PU dispersion (1 : 12) (PU binder)	5/4000, 10/6000, 15/9000
Palmitic acid in 1-propanol (50 mg of palmitic acid/ 1 mL of 1-propanol)	5/800, 10/2200

In the first step, oxygen plasma treated HDPE disks were coated with waterborne polyurethane dispersion (WF 28-453, Stahl), which was diluted with ion-exchanged water in mass ratio of 1 : 1. Polyurethane coating was produced with a spin coater (Laurell WS-400B-6NPP-LITE, North Wales, PA), and the diluted polyurethane dispersion (0.3 mL) was placed on the middle of the sample disks and spin coated. Polyurethane film was cured in an oven at 60°C for 1 h. This layer is referred to below as the protective PU coating.

In the second step, two layers of titanium dioxide were added to the protective PU coating. A suspension containing 2 wt % of TiO_2 was prepared from ion-exchanged water and nanosized Degussa P25 TiO_2 powder (Sachtleben, Germany). The primary particle size of P25 powder is about 26 nm and it consists of anatase and rutile phases (19% of rutile and 81% of anatase).[41] As solid powder, nanoparticles form both agglomerates and aggregates and ultrasonication can be used to disperse agglomerates in liquids but they cannot be broken to primary size particles.[42,43] To disperse TiO_2 agglomerates in ion-exchanged water, the TiO_2 suspension was ultrasonicated for 80 min (Finnsonic m03, Lahti, Finland). Ultrasonicated suspension (0.3 mL) was injected onto the middle of sample disks covered with protective PU coating and spin coated. Samples were dried in an oven for 10 min at 60°C. The second TiO_2 layer was applied in the same way.

In the third step, the immobilized TiO_2 powder was fixed with PU dispersion that was diluted with ion-exchanged water in mass ratio of 1 : 12 (PU dispersion/water). 30 μL of diluted solution was spread evenly on the sample surface and spin coated at high speed to force it into free spaces between the TiO_2 particles. The binding agent was cured in the oven at 60°C for 1 h. This layer will be referred to as the PU binder.

After curing of the binder, some of the samples was treated with oxygen plasma. Treatment time was 10 s, and etching power was set at 300 W.

Working pressure in the chamber was ~ 80 mTorr and oxygen flow was 20 SCCM.

TiO_2 content on sample surfaces

The amount of titanium in samples was determined at Neste Oil, Technology Center, Porvoo, Finland. Samples were burned and ashed at 525°C. The ash was melted at 950°C into a mixture of lithium metaborate and lithium tetraborate, and the melt was dissolved in hydrochloric acid (1 part acid and 10 parts nonionic water). The amount of titanium was determined by inductively coupled plasma spectrometry (ICP). The results were 160 and 170 mg Ti/kg sample for parallel samples, which corresponds to 0.170 mg and 0.180 mg of TiO_2 in the samples (sample masses were 0.6351 and 0.6344 g). Density (ρ) of Degussa P25 titanium dioxide powder is 3.8 g/cm^3, so the volume (V) of TiO_2 was 4.461×10^{-5} cm^3. If the thickness of TiO_2 is assumed to be uniform and the radius of the sample disk is 1.2 cm, the thickness of the TiO_2 film can be calculated by using the equation for cylinder volume. Thicknesses of TiO_2 films in samples were 99 and 105 nm.

Photocatalytic activity studies

Samples were coated with palmitic acid (99%, Aldrich, Steinheim) for photocatalytic studies. Palmitic acid was dissolved in 1-propanol (reagent grade, 99.5%, Labscan, Dublin, Ireland) to a concentration of 50 mg/mL, and the solution was used immediately after preparation. The solution (0.3 mL) was injected on the sample surface and spin-coated, and the solvent was left to evaporate before the UV radiation experiments and contact angle measurements. In the UV radiation experiments, samples were irradiated (UVP Black Ray B100AP, Upland, CA) for 3–18 h (maximum wavelength 365 nm). The distance of the lamp from the sample surface during irradiation was 15 cm.

Water contact angle measurements

Static water contact angles (CA) were determined with a Cam 200 contact angle meter with automatic liquid dispenser (KSV Instruments, Helsinki, Finland). Experiments were carried out at room temperature (~ 22°C) with ion-exchanged water. A water droplet (4 μL) was carefully placed on the sample surface and imaged with the CCD camera once a second for 30 s. The contact angle was determined mathematically by fitting a Young-Laplace curve around the drop. Reported apparent contact angles are averages of five contact angle values determined after stabilization of 30 s.

FTIR-ATR measurements

FTIR-ATR measurements were done with a Digilab FTS 7000 Series Stingray FTIR imaging spectrometer. The spectrometer was coupled with a Digilab UMA 600 infrared microscope containing a mercury cadmium telluride detector. The micro-ATR crystal was a Ge crystal with slide-on ATR adapter. Spectra were collected and processed with Digilab Resolutions Pro 4.0 software. For measurements, 0.3 mL of palmitic acid solution (50 mg palmitic acid/1 mL of 1-propanol) was placed on the sample surface and spin-coated. The sample consisted of oxygen plasma treated HDPE substrate (30 s at 200 W), protective PU coating, and two layers of TiO_2 with plasma treated PU binder (10 s at 300 W). Solvent was evaporated in an oven for 1 h at 45°C and the sample was measured by FTIR-ATR method.

Gas chromatography measurement of palmitic acid residues

Gas chromatography experiments were carried out with an HP 6890 gas chromatograph equipped with an HP 7683 automatic liquid sampler. The chromatograph was connected to a PC running Agilent ChemStation Rev. A.10.01 software. The column was a capillary column HP-5 (length 30 m × i.d. 0.32 mm × film thickness 0.25 μm).

Palmitic acid was rinsed off from samples and, before measurement, was derivatized to trimethylsilyl ester with silylating reagent (Mixture Fluka III, Fluka Chemie, Buchs). Stearic acid (99%, Sigma, Steinheim) was added as internal standard (ISTD). The derivatization process is described elsewhere.[40]

GC measurement was done with temperature programming. Temperatures of the injector and detector were 300 and 315°C, respectively. The sample volume injected was 5 μL, and the injection was done automatically with an autosampler. The heating program for the oven was 120°C for 4 min, increasing 8°C/min up to 300°C, and 300°C for 13.5 min. Retention times were 17.4 min for palmitic acid derivative and 19.7 min for stearic acid derivative (ISTD). Data were analyzed with Agilent ChemStation Rev. A.10.01 software.

Scanning electron microscopy analysis of surfaces

The samples were studied with a Hitachi S4800 FESEM, equipped with upper and lower secondary electron detectors. Samples were cut by using a fretsaw and cross section surfaces of the samples were measured in a vertical position. The samples were attached onto the sample holder with copper adhesive tape and coated with Au (3 nm). An accelerating voltage of 3 kV was applied, and the general

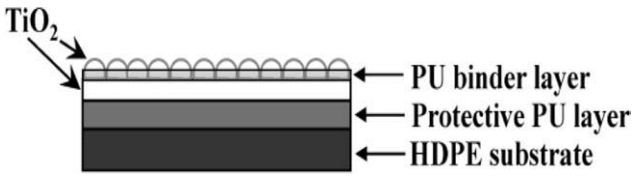

Figure 1 Multilayer structure of the photocatalytic coating on HDPE.

working distance was 8 mm during the SEM imaging.

Mini-SIMS measurements

Mini-SIMS measurements were made with a Millbrook Mini-SIMS spectrometer (Millbrook Instruments, Blackburn, England) equipped with quadrupole mass analyzer. In Mini-SIMS the sample surface is bombarded by high energy $^{69}Ga^{+}$ ions and that leads to the ejection of both neutral and charged (+/−) species from the surface. These ejected species may include atoms, clusters of atoms, and molecular fragments. These species can be detected with mass analyzer. Parameters of Mini-SIMS measurements were mass range 2–200 amu, step of 0.2 amu, and dwell time 0.01 s. Small area sweep mode (225 μm × 225 μm) with charge compensation system was used because of the insulating HDPE substrate. One scan was collected using positive measuring mode. Spectra were analyzed with Millbrook Chemical Microscope software V 2.0.

Optical microscopy imaging of palmitic acid dispersion

Dispersion of palmitic acid was studied with using Olympus BX51 research microscope equipped with Olympus E-330 micro imaging system (E-330M1.2X, Olympus Corp., Japan, Tokyo). Circular polarizer filter (Olympus T2) was applied to detect dispersion of palmitic acid that is seen as interference colors.

RESULTS AND DISCUSSION

Effect of oxygen plasma treatment of HDPE substrate

The multilayered coating on a HDPE substrate consisted of a protective polyurethane (PU) film, and two layers of TiO_2 nanoparticles bound with PU (Fig. 1).

The primary function of the protective PU layer is to prevent direct contact of the substrate with the photocatalytic TiO_2 powder. A second function is to assist dispersion of the photocatalytic powder. Unlike HDPE, the cured PU dispersion is hydrophilic, so the hydrophilic TiO_2 suspension in water is better dispersed on the cured PU surface than on the bare HDPE substrate.

In this study, we found that compatibility between the HDPE substrate and the PU layer is inadequate, resulting in poor adhesion of the PU coating. As shown in Figure 2(A), immersion of the cured protective PU on HDPE in water for 15–30 s caused self-wrinkling of the PU film probably due to stress caused by the water. Because of the poor adhesion, the PU film could even be peeled off. As the water evaporated from the surface, the film smoothened out, but its adhesion to the HDPE remained poor.

The substrate had to be treated, therefore, either chemically or physically, to ensure adequate adhesion of the protective PU. The solution we arrived at was oxygen plasma treatment of the HDPE substrate. The plasma treatment of the HDPE roughens the surface because of selective etching in which amorphous phase is being etched faster than the crystalline phase.[44] The plasma interacts with HDPE leading to carbon–carbon bond scissions and creates

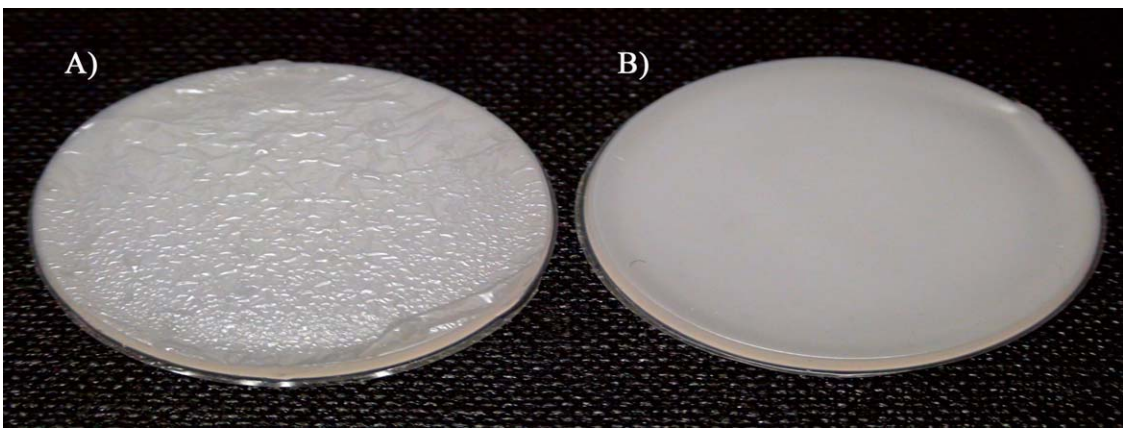

Figure 2 Photographs of the HDPE/PU surface after immersion in water. (A) HDPE substrate with PU coating without oxygen plasma treatment, (B) HDPE substrate treated with oxygen plasma for 30 s at 200 W and then PU coated.

TABLE II
Water Contact Angles, with Standard Deviations, on Different HDPE Substrate Surfaces

Sample code	Composition of sample	Contact angle (°)
S1	HDPE	97 ± 2
S2	HDPE + protective PU	49 ± 3
S3	HDPE + protective PU + TiO_2 + PU binder + palmitic acid	87 ± 2
S4	Plasma-treated HDPE	50 ± 3
S5	Plasma-treated HDPE + protective PU	55 ± 1
S6	Plasma-treated HDPE + protective PU + TiO_2 + PU binder + palmitic acid	82 ± 3

oxygen-containing hydrophilic functional groups (e.g., C=O and COOH) on the HDPE surface.[45] Plasma treated (30 s at 200 W) surface of HDPE becomes hydrophilic observed as a decrease in water contact angle from 97° (S1) to 50° (S4) (Table II).

Plasma treatment changes HDPE surface chemically more compatible with hydrophilic protective PU layer. Improved adhesion between the substrate and PU film is indicated by the absence of self-wrinkling when HDPE/PU system is immersed in water [Fig. 2(B)].

Improved adhesion between the HDPE substrate and protective PU coating also enhances spreading and dispersion of TiO_2 on the protective PU surface (Fig. 3). Figure 3 shows SEM images of two samples in which HDPE/PU system has been coated with TiO_2. In Figure 3(B), the PU film is still firmly adhered to the HDPE surface due to better adhesion induced by plasma treatment of the substrate. From Figure 3(B), we can observe that TiO_2 dispersion is more uniform compared to the sample in Figure 3(A), which has not undergone plasma treatment. Moreover, in the sample of Figure 3(A), the PU/TiO_2 layer was detached from the HDPE substrate during the sample preparation indicating a very poor adhesion between the untreated substrate and the protective PU coating.

Effect of oxygen plasma treatment of PU binder

We studied the effect of plasma treatment of the PU binder on the photocatalytic activity of TiO_2 bound with PU. Using Mini-SIMS, we measured the amount of TiO_2 available on the surface before and after oxygen plasma treatment of the binder layer. At the same time, changes in the hydrophilic/hydrophobic nature of the samples were followed with CA measurements, and degradation of palmitic acid was monitored by GC. In previous work,[40] we found photocatalytic activity to be weak when the PU binder was not plasma treated; only ~ 16% of palmitic acid decomposed. At that time, the effect of plasma treatment of the HDPE surface was not studied.

Mini-SIMS allows monitoring of the surface for specific secondary ions of elements and their molecules. When the PU binder is etched, it is likely that more titanium will be exposed, and this can be measured by Mini-SIMS as amount of titanium ions. Three HDPE samples were tested: one with PU binder, one with oxygen plasma treated (10 s at 300 W) PU binder and one without PU binder. Cations Ti^+ (*m/z* 48) and TiO^+ (*m/z* 64) were monitored and results are reported in Table III.

Small area sweep (225 μm × 225 μm) was used in the Mini-SIMS measurements because point mode may cause excessive erosion. As can be seen in Table III, oxygen plasma treatment of PU binder had a clear effect on the sample surface: more titanium was detected when the binder was plasma etched. Intensities (cps) were highest for samples without PU binder. Variation was wide between the

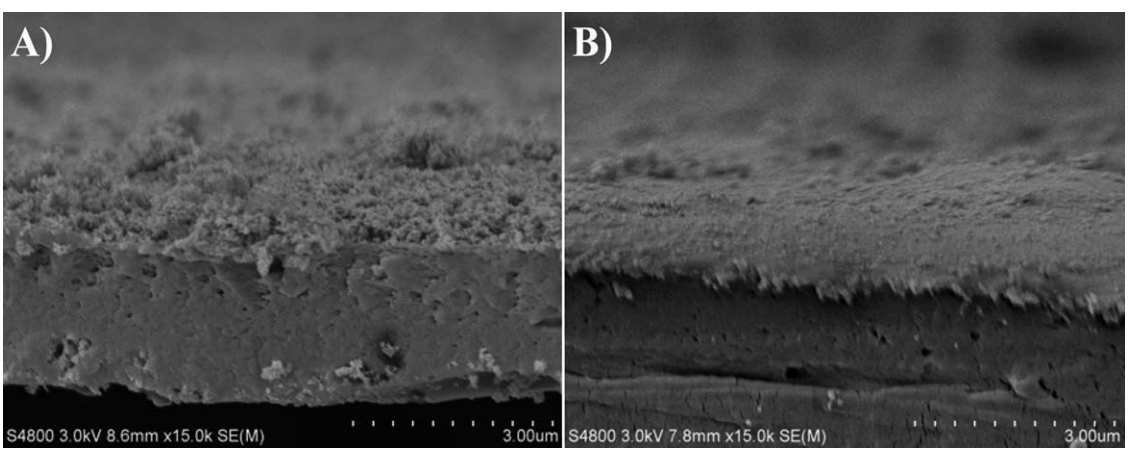

Figure 3 SEM images of the PU/TiO_2 surfaces. (A) PU coating without oxygen plasma treatment of HDPE substrate, (B) HDPE substrate treated with oxygen plasma for 30 s at 200 W and then PU coated. Magnification in images is 15 k.

TABLE III
Amounts of Titanium-based Cations (Average of Three Measurements) Determined by Mini-SIMS

Sample composition	cps (Ti^+ m/z 47.8–48.2)	cps (TiO^+ m/z 63.8–64.2)
Plasma-treated HDPE + protective PU + TiO_2 + PU binder	23,700	6700
Plasma-treated HDPE + protective PU + TiO_2 + plasma-treated PU binder	28,700	10,500
Plasma-treated HDPE + protective PU+TiO_2	38,700	13,200

measurement areas owing to the sensitivity of the method, but the overall trend is clear.

The effect of oxygen plasma treatment of PU binder on the hydrophilic properties of TiO_2 containing surfaces was studied by water contact angle (CA) measurements. This method was also applied for monitoring the changes in hydrophilicity when palmitic acid was added on some samples as a model soil and then photocatalytically decomposed by UV irradiation (see below). Table IV presents measured CA values for HDPE samples where the PU binder was not and was plasma treated.

As can be seen in Table IV, for samples that contained TiO_2 but no palmitic acid, plasma treatment of the PU binder causes a significant lowering of the water contact angle, from 55° (CA1 without plasma treatment) to 0° (CA4 with plasma treatment). In other words, the sample surface becomes superhydrophilic. Application of palmitic acid to the sample surfaces causes an increase in the water contact angle: without oxygen plasma treatment of the PU binder, the contact angle increases by 34° (cf. CA1 and CA2), and with plasma treatment by 46° (cf. CA4 and CA5). In both cases, UV irradiation of 3 h causes a clear decrease in the water contact angle, but superhydrophilicity is not obtained, indicating that only part of the palmitic acid has degraded.

The standard deviations in CA values are high for samples CA5 and CA6, with plasma treated PU binder and containing palmitic acid. Plasma treatment of PU binder creates polar groups and increased hydrophilicity[45] observed as lower CA values. For its part, palmitic acid tends to crystallize and form islands,[46] making the surface system unstable and causing wide deviations in the contact angles of samples CA5 and CA6.

The extent of degradation of palmitic acid after 3 h UV irradiation was studied by GC for a set of HDPE samples (plasma-treated HDPE + protective PU + TiO_2 + PU binder + PA) prepared without and with plasma treatment (10 s at 300 W) of PU binder. According to the GC results, the average amount of palmitic acid after 3 h UV irradiation was 43.5 μg (37.5–47.5 μg) for nontreated and 43.3 μg (41.8–45.1 μg) for plasma-treated samples. Relative to a reference sample (115.7 μg) without UV irradiation, ~ 37% of palmitic acid was left, indicating that 3 h UV irradiation degrades palmitic acid only partially. This is consistent with the CA results.

We conclude from these results that, if the HDPE substrate is oxygen plasma treated before dispersion of protective PU coating, TiO_2 photocatalysis works well even without oxygen plasma treatment of the PU binder. According to SIMS measurements, some of the PU binder is etched off in plasma treatment of the binder, and that does not improve the photocatalytic efficiency when UV irradiation time is only a few hours. Moreover, plasma treatment of PU

TABLE IV
Results of Water CA Measurements, with Standard Deviations, for Samples Where the PU Binder Was and Was Not Plasma Treated

Sample code	Plasma treatment of PU binder [time (s)/power (W)]	Contains palmitic acid	UV irradiation time (h)	Contact angle of water (°)
CA1	0/0	No	0	55 ± 3
CA2	0/0	Yes	0	89 ± 2
CA3	0/0	Yes	3	31 ± 7
CA4	10/300	No	0	Super hydrophilic
CA5	10/300	Yes	0	46 ± 15
CA6	10/300	Yes	3	39 ± 12

All samples consisted of plasma-treated HDPE substrate (30 s at 200 W), protective PU coating and two layers of TiO_2 and PU binder.

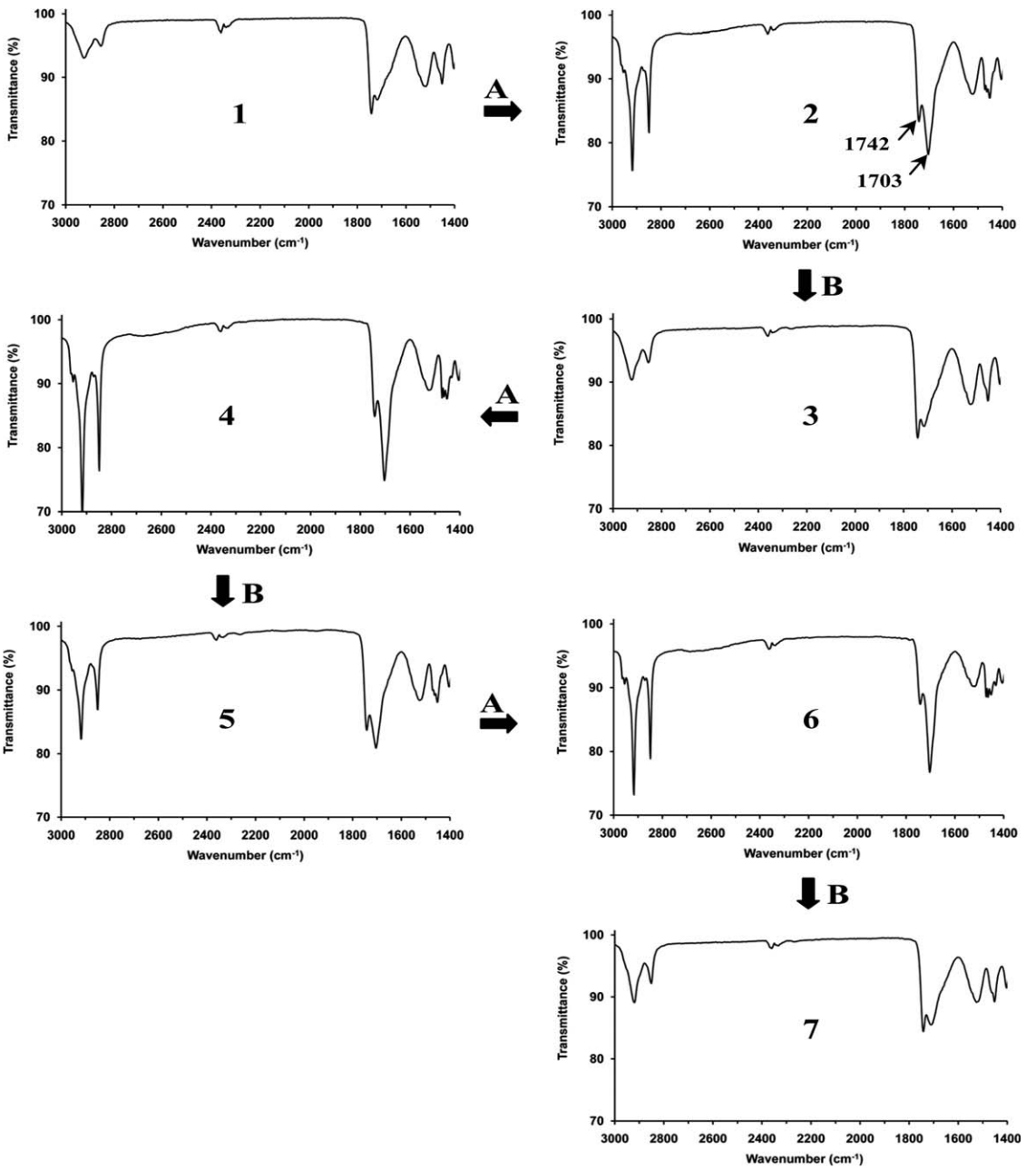

Figure 4 FTIR spectra of a sample consisting of plasma-treated HDPE substrate (30 s at 200 W), protective PU coating, two layers of TiO_2, and plasma-treated PU binder (10 s at 300 W). A indicates addition of palmitic acid and B 6 h UV irradiation.

binder may have a negative effect on fixing of TiO_2 particles.

Long-term activity of TiO_2 in degradation of palmitic acid

FTIR-ATR is a fast and simple method for monitoring the long-term activity of TiO_2. We used palmitic acid as a test compound in our experiments, measuring the intensity of its carbonyl vibration before and after three degradation cycles.

The carbonyl vibration of palmitic acid is strong and sharp ($\sim$ 1703 cm^{-1}), but it must be noted that polyurethane contains carbonyl group in the urethane group, so there is some overlap between the different carbonyl groups. Strong C—H vibrations of palmitic acid are detected at wavenumbers $\sim$ 2848 cm^{-1} and 2916 cm^{-1} and some small C—H vibrations in the range of 1452–1471 cm^{-1}, but again there is overlap with the weak C—H vibration of polyurethane.

Figure 4 presents FTIR spectra of a sample on which palmitic acid has been spin coated (A) and the sample has been UV irradiated for 6 h (B). A longer irradiation time was used in this experiment because preliminary tests showed that 3 h irradiation was not

TABLE V
Amounts of Palmitic Acid in Samples Measured by GC

Sample code	UV-irradiation time (h)	Integrals of trimethylsilyl ester of palmitic acid	Integrals of trimethylsilyl ester of stearic acid (ISTD)	Amount of palmitic acid (μg)
GC1	0	589.7	509.6	115.7
GC2	6	64.1	565.8	11.3
GC3	9	30.7	592.7	5.2
GC4	12	15.9	533.7	3.0
GC5	15	22.4	605.8	3.7

All samples consisted of plasma-treated HDPE substrate (30 s at 200 W), protective PU coating, two layers of TiO_2, plasma-treated PU binder (10 s at 200 W) and palmitic acid.

enough to decompose palmitic acid. This cycle was repeated three times. When palmitic acid is added, C—H signals in region $\sim$ 2850–2920 cm^{-1} (Spectrum 2) strengthen substantially relative to those of Spectrum 1 where no palmitic acid was added. Also, a new peak appears at 1703 cm^{-1} (carbonyl peak of palmitic acid), while a "shoulder" from PU is still seen at 1742 cm^{-1}. Spectrum 3, recorded after UV irradiation for 6 h, is almost identical with Spectrum 1 but with stronger intensities in regions $\sim$ 2850–2920 cm^{-1} and $\sim$ 1720–1740 cm^{-1}. The peak at 1703 cm^{-1} in Spectrum 2 has disappeared. We conclude that most of the palmitic acid has been photocatalytically degraded.

After a second identical addition cycle of palmitic acid (Spectrum 4), IR band intensities are higher at 1703 cm^{-1} and in the region $\sim$ 2850–2920 cm^{-1} as compared with those after the first addition (Spectrum 2). Evidently some palmitic acid remains after the first UV cycle (Spectrum 3). Another UV cycle does not remove all the palmitic acid (Spectrum 5). Palmitic acid still degrades, but comparison of the UV cycles indicates that the amount of palmitic acid varies at different measurement points on the sample surface. This is probably due of the formation of palmitic acid islands in the spin coating, so that the palmitic acid on the sample surface is not uniformly decomposed during the UV cycle. The third cycle (Spectra 6 and 7) confirms that the photocatalytic TiO_2 coating still works, but the original state without palmitic acid (Spectrum 1) is not completely restored. Spectrum 7 is nevertheless very similar to Spectrum 3 (after first cycle).

From these findings we conclude that degradation of palmitic acid can be evaluated by FTIR-ATR, but not quantitatively. Another method, such as gas chromatography, is needed to measure the exact amounts of palmitic acid in samples and to confirm the degradation. Important advantages of FTIR-ATR over GC are that tedious derivatization is not required and that samples are not destroyed.

Kinetics of palmitic acid degradation

Our final target was to determine the UV-irradiation time and kinetics for a complete photochemical degradation of palmitic acid. The degradation studies were made on samples in which PU binder of TiO_2 layers was oxygen plasma treated. Our FTIR-ATR measurements indicated that 6 h may not be enough for the total decomposition, and we therefore studied UV-irradiation times of 6, 9, 12, and 15 h (Table V). Palmitic acid residues in UV-illuminated samples were measured by GC analysis and compared with those of an unilluminated reference sample.

The results in Table V confirm that 6 h is insufficient for complete photocatalytic decomposition of palmitic acid. Within 6 h 90% of palmitic acid degraded. GC analysis indicated that about 12 h is needed to degrade palmitic acid almost completely (only 2.6% of palmitic acid left).

Degradation kinetics of the disappearance of saturated fatty acids such as palmitic acid[47] or stearic acid[48] is generally zero-order when TiO_2 is the photocatalyst. However, when the amount of fatty acids is extremely limited, as in stains[49] or Langmuir-Blodgett films (thickness of fatty acid film $\sim$ 12.5 nm),[50] the degradation kinetics is exponential (pseudofirst order). In this study, the initial amount of palmitic acid was 115.7 μg (25.6 $\mu g/cm^2$), and TiO_2 nanocoating about 100 nm thick was applied as a photocatalyst layer to effect the decomposition of palmitic acid. When the amount of palmitic acid is plotted as a function of UV-irradiation time, using the GC results from Table V and the result obtained from GC analysis after 3 h (43.5 μg, determined in the study on effect of oxygen plasma treatment of PU binder), it is clear [Fig. 5(A)] that the degradation kinetics is not zero-order. For a pseudofirst-order reaction we can write $[PA]_t = [PA]_0 \exp(-k_{obs}t)$ or $\ln([PA]_0/[PA]) = k_{obs}t$, where $[PA]_t$ and $[PA]_0$ are the concentrations of palmitic acid at time t and *0*, respectively, and k_{obs} is the pseudo-first-order rate constant. When the natural logarithm

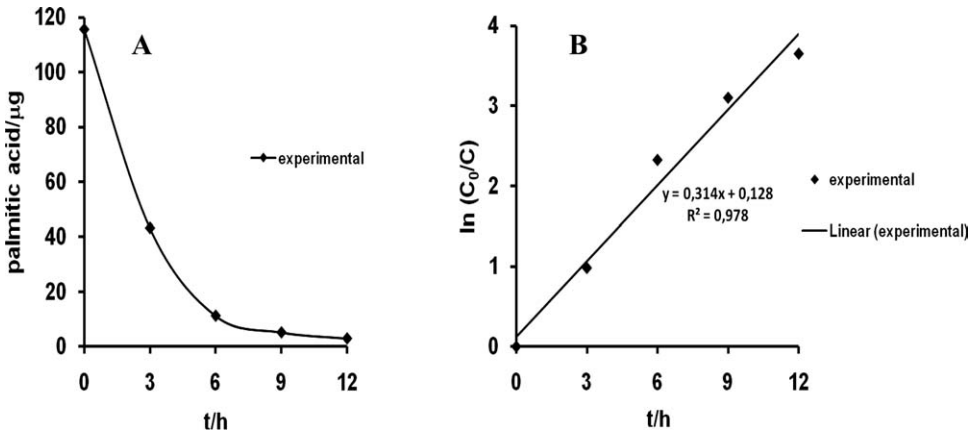

Figure 5 Concentration of palmitic acid plotted as a function of UV-irradiation time (A), and natural logarithm of concentration as a function of UV-irradiation time (B). Samples as described in Table V consisted of plasma-treated HDPE substrate (30 s at 200 W), protective PU coating, two layers of TiO_2, plasma-treated PU binder (10 s at 200 W) and palmitic acid.

of ($[PA]_0/[PA]$) is plotted as a function of reaction time, t, the dependence is almost linear [Fig. 5(B)], indicating pseudofirst-order kinetics. From Figure 5(B), we obtain the rate constant $k_{obs} = 0.31\ h^{-1}$ ($R^2 = 0.98$).

From Figure 5(A), it appears that the degradation kinetics of palmitic acid is initially zero-order (nearly linear from 0 to 6 h, $k_{obs} = 17.4\ \mu g\ h^{-1} = 0.068\ \mu mol\ h^{-1}$), but the reaction rate changes as UV irradiation is continued. It has been reported for stearic acid

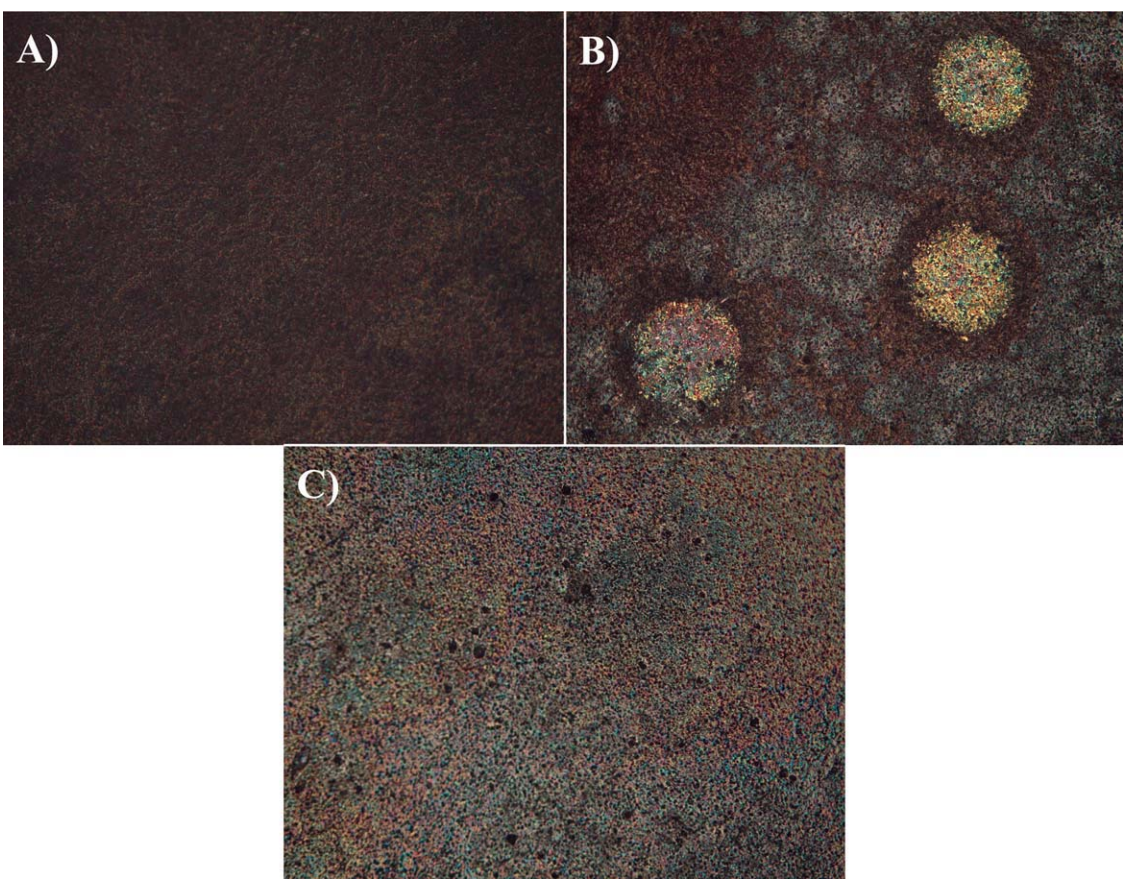

Figure 6 Stereomicroscopic images of the TiO_2 containing surfaces before and after addition of palmitic acid. (A) TiO_2/PU binder surface without palmitic acid, (B) TiO_2/PU binder surface with palmitic acid, and (C) TiO_2/PU binder surface with palmitic acid. In samples A and B PU binder is oxygen plasma treated for 10 s at 300 W. Magnification in images is ×12. [Color figure can be viewed in the online issue, which is available at wileyonlinelibrary.com.]

that the layer thickness affects the degradation kinetics: thin films decay exponentially (pseudofirst order) and thicker films degrade more slowly.[49] Sawunyama et al.[50] found that decomposition of stearic acid is an inhomogeneous process and that degradation occurs randomly throughout the fatty acid film. They also noticed that stearic acid may aggregate when photodecomposition is initiated. Since palmitic acid is chemically very similar to stearic acid, it is likely that it, too, decomposes in an inhomogeneous manner.

In our samples palmitic acid is spread on a uniform surface of titanium dioxide, which has been bound with PU and oxygen plasma treated. A stereomicroscopic image of palmitic acid layer before UV irradiation in Figure 6(B) shows that it forms both large and small islands, which are seen as interference colors. However, a featureless image of the TiO_2 surface in Figure 6(A) indicates a uniform topography of titanium dioxide particles. The inhomogeneous dispersion of palmitic acid affects both surface topography and wettability properties, which were observed as wide deviations in water contact angles (samples CA5 and CA6 in Table IV). The uneven distribution of palmitic acid is probably due to the plasma treatment of titanium dioxide/PU surface, since when palmitic acid is on nonplasma-treated TiO_2 surface it does not form islands [Fig. 6(C)]. We conclude that oxygen plasma treatment of the titanium dioxide/PU layer renders its functionality, which causes island formation of palmitic acid and its degradation by pseudofirst-order reaction kinetics.

CONCLUSIONS

A photocatalytically active, self-cleaning TiO_2-based multilayer structure was prepared on HDPE substrate. Adhesion between the protective PU coating and HDPE substrate was successfully improved by oxygen plasma treatment of the substrate. Oxygen plasma treatment increases the surface energy of HDPE, seen as decreasing contact angle of water, to near the pure PU contact angle. Without oxygen plasma treatment it is almost impossible to obtain adequate adhesion between HDPE substrate and the protective PU coating. Poor adhesion leads to tensions in the protective PU coating, and to wrinkling, when TiO_2 and PU binder are added. Photocatalytic activity is substantially deteriorated as a consequence.

FTIR-ATR method was successfully applied with GC analysis in study of the degradation of palmitic acid. It was shown that the photocatalytic multilayer coating is effective through several cycles, and degradation can be detected by FTIR-ATR. It must be noted that the carbonyl absorption bands of PU and palmitic acid are overlapping and the FTIR-ATR method should be used for qualitative analysis only. FTIR-ATR measurements showed that palmitic acid degraded almost completely in 6 h, but according to GC analysis complete degradation takes $\sim$ 12 h (97.4% of palmitic acid was degraded in 12 h).

Plasma treatment of the PU binder had no significant effect on the activity of samples. From Mini-SIMS measurements, it appears that oxygen plasma treatment etches off some of the PU binder, but degradation of palmitic acid occurs at the same rate whether the sample is plasma treated or not. Photocatalytic activity of TiO_2 was determined for samples where PU binder was plasma treated and, according to the experimental data, degradation kinetics of palmitic acid is pseudofirst-order with a rate constant of 0.31 h^{-1}.

References

1. Fujishima, A.; Honda, K. Nature 1972, 238, 37.
2. Fujishima, A.; Zhang, X.; Tryk, D. A. Int J Hydrog Energ 2007, 32, 2664.
3. Carp, O.; Huisman, C. L.; Reller, A. Prog Solid State Ch 2004, 32, 33.
4. Mills, A.; Le Hunte, S. J Photochem Photobiol A 1997, 108, 1.
5. Linsebigler, A. L.; Lu, G.; Yates, J. T., Jr. Chem Rev 1995, 95, 735.
6. Mills, A.; McFarlane, M. Catal Today 2007, 129, 22.
7. Simonsen, M. E.; Jensen, H.; Li, Z.; Søgaard, E. G. J Photochem Photobiol A 2008, 200, 192.
8. Hoffmann, M. R.; Martin, S. T.; Choi, W.; Bahnemann, D. W. Chem Rev 1995, 95, 69.
9. Buxbaum, G.; Pfaff, G., Eds. Industrial Inorganic Pigments, 3rd ed.; Wiley-VCH: Weinheim, 2005; p 51.
10. Karvinen, S. M. Ind Eng Chem Res 2003, 42, 1035.
11. Allen, N. S.; Edge, M.; Verran, J.; Stratton, J.; Maltby, J.; Bygott, C. Polym Degrad Stabil 2008, 93, 1632.
12. Allen, N. S.; Edge, M.; Ortega, A.; Liauw, C. M.; Stratton, J.; McIntyre, R. B. Polym Degrad Stabil 2002, 78, 467.
13. Sabzi, M.; Mirabedini, S. M.; Zohuriaan-Mehr, J.; Atai, M. Prog Org Coat 2009, 65, 222.
14. Couteau, C.; El-Boury, S.; Paparis, E.; Sébille-Rivain, V.; Coiffard, L. J. M. Pharm Dev Technol 2009, 14, 369.
15. Tobaldi, D. M.; Tucci, A.; Camera-Roda, G.; Baldi, G.; Esposito, L. J Eur Ceram Soc 2008, 28, 2645.
16. Al-Ekabi, H.; Serpone, N. J Phys Chem 1988, 92, 5726.
17. Tennakone, K.; Tilakaratne, C. T. K.; Kottegoda, I. R. M. Water Res 1997, 31, 1909.
18. Behnajady, M. A.; Modirshahla, N.; Mirzamohammady, M.; Vahid, B.; Behnajady, B. J Hazard Mater 2008, 160, 508.
19. Belapurkar, A. D.; Sherkhane, P.; Kale, S. P. Curr Sci 2006, 91, 73.
20. Carneiro, J. O.; Teixeira, V.; Portinha, A.; Magalhães, A.; Coutinho, P.; Tavares, C. J.; Newton, R. Mater Sci Eng B 2007, 138, 144.
21. Tennakone, K.; Tilakaratne, C. T. K.; Kottegoda, I. R. M. J Photochem Photobiol A 1995, 87, 177.
22. Zhiyong, Y.; Mielczarski, E.; Mielczarski, J.; Laub, D.; Buffat, Ph.; Klehm, U.; Albers, P.; Lee, K.; Kulik, A.; Kiwi-Minsker, L.; Renken, A.; Kiwi, J. Water Res 2007, 41, 862.
23. Zhiyong, Y.; Laub, D.; Bensimon, M.; Kiwi, J. Inorg Chim Acta 2008, 361, 589.
24. Naskar, S.; Pillay, S. A.; Chanda, M. J Photochem Photobiol A 1998, 113, 257.

25. Essawy, A. A.; El-Hag Ali, A.; Abdel-Mottaleb, M. S. A. J Hazard Mater 2008, 157, 547.
26. Dhananjeyan, M. R.; Kiwi, J.; Thampi, K. R. Chem Commun 2000, 15, 1443.
27. Matsuzawa, S.; Maneerat, C.; Hayata, Y.; Hirakawa, T.; Negishi, N.; Sano, T. Appl Catal B-Environ 2008, 83, 39.
28. Fostier, A. H.; do Socorro Silva Pereira, M.; Rath, S.; Guimarães, J. R. Chemosphere 2008, 72, 319.
29. Bozzi, A.; Yuranova, T.; Kiwi, J. J Photochem Photobiol A 2005, 172, 27.
30. Meilert, K. T.; Laub, D.; Kiwi, J. J Mol Catal A Chem 2005, 237, 101.
31. Chen, F.; Yang, X.; Wu, Q. Build Environ 2009, 44, 1088.
32. Fujishima, A.; Hashimoto, K.; Watanabe, T. TiO_2 Photocatalysis. Fundamentals and Applications, 1st ed.; BKC: Tokyo, 1999; pp 46–114.
33. Fujishima, A.; Zhang, X.; Tryk, D. A. Surf Sci Rep 2008, 63, 515.
34. Zhao, X.; Li, Z.; Chen, Y.; Shi, L.; Zhu, Y. J Mol Catal A-Chem 2007, 268, 101.
35. Zhao, X.; Li, Z.; Chen, Y.; Shi, L.; Zhu, Y. Appl Surf Sci 2008, 254, 1825.
36. Duffy, E. F.; Al Touati, F.; Kehoe, S. C.; McLoughlin, O. A.; Gill, L. W.; Gernjak, W.; Oller, I.; Maldonado, M. I.; Malato, S.; Cassidy, J.; Reed, R. H.; McCuigan, K. G. Sol Energy 2004, 77, 649.
37. Negishi, N.; Takeuchi, K.; Ibusuki, T. J Mater Sci Lett 1999, 18, 515.
38. Xiang, J.; Masuda, Y.; Koumoto, K. Adv Mater 2004, 16, 1461.
39. Schmidt, H.; Naumann, M.; Müller, T. S.; Akarsu, M. Thin Solid Films 2006, 502, 132.
40. Kasanen, J.; Suvanto, M.; Pakkanen, T. T. J Appl Polym Sci 2009, 111, 2597.
41. Raj, K. J. A.; Viswanathan, B. Indian J Chem A 2009, 48, 1378.
42. Mandzy, N.; Grulke, E.; Druffel, T. Powder Technol 2005, 160, 121.
43. Jiang, J.; Oberdörster, G.; Biswas, P. J Nanopart Res 2009, 11, 77.
44. Olde Riekerink, M. B.; Terlingen, J. G. A.; Engbers, G. H. M.; Feijen, J. Langmuir 1999, 15, 4847.
45. Drnovská, H.; Lapčik L., Jr.; Buršiková, V.; Zemek, J.; Barros-Timmons, A. M. Colloid Polym Sci 2003, 281, 1025.
46. Tikka, H.-K.; Suvanto, M.; Pakkanen, T. A. J Colloid Interface Sci 2004, 273, 388.
47. Roméas, V.; Pichat, P.; Guillard, C.; Chopin, T.; Lehaut, C. New J Chem 1999, 23, 365.
48. Mills, A.; Lepre, A.; Elliott, N.; Bhopal, S.; Parkin, I. P.; O'Neill, S. A. J Photochem Photobiol A 2003, 160, 213.
49. Vicente, J. P.; Gacoin, T.; Barboux, P.; Boilot, J.-P.; Rondet, M.; Guéneau, L. Int J Photoenergy 2003, 5, 95.
50. Sawunyama, P.; Jiang, L.; Fujishima, A.; Hashimoto, K. J Phys Chem B 1997, 101, 11000.